# 11.5 COLD-AIR POOL DETECTION TOOLS IN THE PYRENEES VALLEYS

Josep R. Miró *(1); Meritxell Pagès(1); Meinolf Koßmann(2)
(1) Meteorological Service of Catalonia, Barcelona (Spain)
(2) Deutscher Wetterdienst, Offenbach (Germany)

## 1. ABSTRACT

The aim of this study is to classify the different valleys within the Pyrenees range using different methods to be later combined for obtaining the most likely areas where cold-air pool (CAP) events can be observed.

Since the Pyrenees Range has a high number of valleys and basins, the Segre River Valley (Catalonia, Spain) was chosen to carry out the study. Its classification derived through several techniques is presented here.

Firstly, field observations from AWS have been used for statistical analysis based on regression, cluster and Empirical Orthogonal Functions (EOF) (Lundquist & Cayan., 2007).

Secondly, the effects of nocturnal down-valley flows have been studied in more detail using a drainage wind model (KLAM_21 operated by the Deutscher Wetterdienst) as well as evaluations of the Topographical Amplification Factor (TAF) and several topographic tools (Lundquist et Al., 2008) .

Finally, from the combination of all techniques an idea about the cold air behavior has been elaborated in relation to the CAP within the Segre river valley.

## 2. INTRODUCTION

Temperatures are especially unpredictable in some complex orography areas, mainly in calm and clear nights where the synoptic situations show a ridge aloft and a weak high pressure gradient in surface. Thus, temperature inversions are observed and this difficults the temperature forecasts, both horizontally and vertically.

The numerical models show strong limitations in either synoptic or mesoscale scales in mountain zones, and downscaling methods are needed to improve the results.

Several possibilities can improve the temperature forecast, whether these use statistic or dynamic downscaling, both with disadvantages and compensations.
The statistic methods need large amounts of AWS' data that in complex terrain are only punctual values, which do not represent the area. On the other hand, the dynamic downscaling is very expensive when computing and its results are more qualitative than quantitative.

For this reason a new method is proposed in order to classify the places where the use of microscale numerical model is needed and where the AWS are representative.

The classification will be based on the places where is likely the cold air pooling.

A portion of the River Segre Valley was chosen, in particular the area from Cerdanya region to Oliana in the Alt Urgell, region that comprises basins and canyons together with high peaks that almost reach 3000 meters.

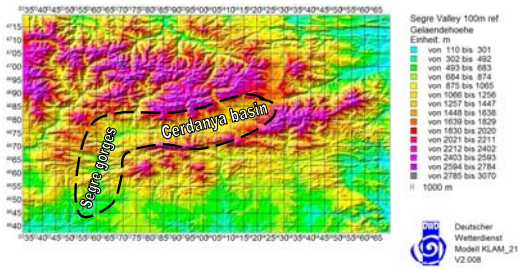


Figure 1.Topography of the study area

## 3. DATA

Several minimum temperature data sets from AWS within the valley (Table 1) were used on the statistical methods, since November 2003 to March 2005.

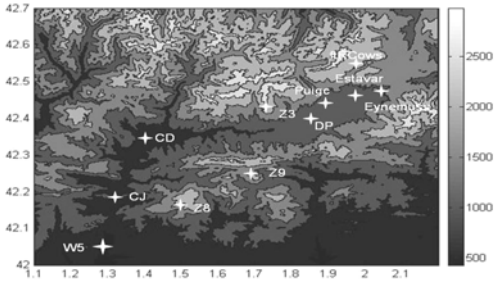


Figure 2. AWS location map

*Corresponding author address: Josep R. Miró
Meterological Service of Catalonia, Barcelona, Spain;
email: jrmiro@meteo.cat

| AWS | AWS CODE | ALTITUDE (m) | OWNER | TYPE |
|---|---|---|---|---|
| Oliana | W5 | 506 | SMC | BVAWS |
| Organyà | CJ | 566 | SMC | BVAWS |
| La Seu d'Urgell | CD | 849 | SMC | IAWS |
| Das | DP | 1.097 | SMC | BVAWS |
| Puigcerdà | Puigc | 1.210 | Aemet | BVAWS |
| Estavar | Estavar | 1.268 | U.P.(UK) | BVAWS |
| Eyne | EyneMus | 1.559 | U.P.(UK) | IAWS |
| Font Romeu | FtrCows | 2.111 | U.P.(UK) | HMAWS |
| Cadí Nord | Z9 | 2.149 | SMC | HMAWS |
| Port del Comte | Z8 | 2.300 | SMC | HMAWS |
| Malniu | Z3 | 2.310 | SMC | HMAWS |

Table 1. SMC: Servei Meteorològic de Catalunya; AEMet: Agencia Estatal de Meteorología; U.P. (UK): University of Portsmouth.

The AWS were classified in three groups since they are located on different heights (Figure 2) and terrain shapes. Hence, high mountain AWS (HMAWS), those up to 1800 meters bottom valley AWS (BVAWS) those on the lower sites within the valley, and intermediate AWS (IAWS) those below 1800 meters and settled on the slopes

## 4. METHODS

Two methods were used focused on distinguishing the areas where CAP develops. Firstly, the statistic tools such as correlations ($R^2$), clusters and Empirical Orthogonal Functions (EOF), and secondly tools based on drainage studies like the Topographic Amplification Factor (TAF) and a drainage model (KLAM_21).

### *4.1 Statistic methods*

By means of correlations and clusters, it was found a first idea about differences and similarities on the behavior of the minimum temperatures among AWS. On the other hand, it was very useful to look into EOF to detect sites with high or low likelihood of CAP.

*Correlations $R^2$*

Due to the major CAP events occur in winter, only the cold months data have been used to detect extreme correlation values. Using the whole data the correlation values were unremarkable and so does not imply significant changes in the results.

HMAWS are a homogeneous group and there is an important correlation among them (> 0,90) (Table 2). Thus, AWS settled upper 1800 m act together as the free atmosphere (Pagès i Miró, 2009) concerning to the temperature values. However, the correlations between HMAWS and the others AWS show considerably lower values (e.g. $R^2$= 0,11) even if they are close in a horizontal plane, like happens between DP and Z3 (see Figure 2). On the other hand, BVAWS and IAWS correlation values show extreme differences among them with clearly lower values than HMAWS which range from 0,48 to 0,86.

Despite the insignificant correlation values between HMAWS and the others, it is interesting to see that EyneMus, Estavar, Puigc and CD show higher correlation values than the rest. The higher values are normal for EyneMus and CD as these are IAWS, but the remarkable values of Puigc and Estavar mean that despite they are BVAWS without likelihood of CAP events, probably due to drainage.

| | Z3 | Z8 | Z9 | ftRCows | EyneMus | Estavar | Puigcerdà | DP | CD | CJ | W5 |
|---|---|---|---|---|---|---|---|---|---|---|---|
| Z3 | 1 | 0,97 | 0,97 | 0,95 | 0,62 | 0,33 | 0,36 | 0,12 | 0,31 | 0,15 | 0,16 |
| Z8 | 0,97 | 1 | 0,96 | 0,95 | 0,60 | 0,32 | 0,35 | 0,11 | 0,30 | 0,15 | 0,15 |
| Z9 | 0,97 | 0,96 | 1 | 0,96 | 0,63 | 0,33 | 0,37 | 0,12 | 0,32 | 0,15 | 0,16 |
| ftRCows | 0,95 | 0,95 | 0,96 | 1 | 0,70 | 0,40 | 0,44 | 0,18 | 0,40 | 0,21 | 0,23 |
| EyneMus | 0,62 | 0,60 | 0,63 | 0,70 | 1 | 0,84 | 0,79 | 0,57 | 0,75 | 0,50 | 0,48 |
| Estavar | 0,33 | 0,32 | 0,33 | 0,40 | 0,84 | 1 | 0,83 | 0,81 | 0,84 | 0,60 | 0,54 |
| Puigcerdà | 0,36 | 0,35 | 0,37 | 0,44 | 0,79 | 0,83 | 1 | 0,73 | 0,84 | 0,62 | 0,56 |
| DP | 0,12 | 0,11 | 0,12 | 0,18 | 0,57 | 0,81 | 0,73 | 1 | 0,86 | 0,75 | 0,63 |
| CD | 0,31 | 0,30 | 0,32 | 0,40 | 0,75 | 0,84 | 0,84 | 0,86 | 1 | 0,80 | 0,71 |
| CJ | 0,15 | 0,15 | 0,15 | 0,21 | 0,50 | 0,60 | 0,62 | 0,75 | 0,80 | 1 | 0,80 |
| W5 | 0,16 | 0,15 | 0,16 | 0,23 | 0,48 | 0,54 | 0,56 | 0,63 | 0,71 | 0,80 | 1 |

Table 2. $R^2$ values

The correlations of DP and EyneMus are singular. The first one shows very low correlation values respect HMAWS when compared with the other BVAWS; the reason could be found in the strong CAP events that take place in.

The others, classified IAWS, seem to be a border between the HMAWS and the other AWS correlation values. The reason is that EyneMus is settled on a slope and it connects two features: high mountain that are coupled with free air circulation and the lower sites that show a more local behavior.

*Clusters*

The aim of using the cluster analysis was to find out how the AWS differ, in other words, how they separate in groups using a fixed distance. In this case, the hierarchical method and the Euclidean distance were used.

The results obtained were represented by dendrograms (Figure 3).

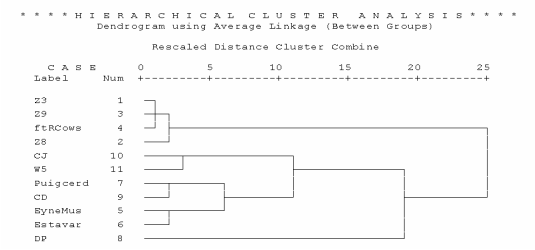


Figure 3. AWS' minimum temperature dendrogram

Looking into the dendrogram, the first division of AWS was the composed by all the HMAWS on the one hand and the other AWS on the other one. In this last group, formed by BVAWS and IMAWS, DP separated first, and later a couple of groups appeared; the first one consists of Organyà (CJ) and Oliana (W5), and the second of the AWS in the Cerdanya, except Das.

Thus, there is a clear difference between the temperature values from the HMAWS and the other ones. Between BVAWS and IMAWS there are several groups in the dendrogram that enhance the importance of characterizing the lower sites, since DP was aisled alone at the beginning and shows a special behavior. On the other hand, the other AWS are joined depending on the valley orientation: from north to south (CJ and W5) and from east to west (CD, Puigc, EyneMus, Estavar).

*Analysis Empirical Orthogonal Function (EOF)*

- *Temperature Classification by EOF*

The EOF analysis decomposes a set of time-space series by means of orthogonal functions:

$$Z(x,y,t) = \sum_{k=1}^{N} PC(t).EOF(x,y)$$

where EOF(x,y) shows the spatial structures (x,y) of the major factors that can account for the temporal variations of Z and PC(t) is the principal component that explains how the amplitude of the EOF varies with time.
The EOF are orthogonal in space and the PCs in time which means that there is no spatial correlation between them.

- *EOF results*

In order to obtain the results it was needed to transform the whole AWS minimum temperature series using:

$$T\left(\vec{x},t\right) = \overline{T}\left(\vec{x}\right) + \overline{T'}\left(t\right) + \widetilde{T}\left(\vec{x},t\right) + \varepsilon$$

where $\overline{T}\left(\vec{x}\right)$ is the mean annual minimum temperature (height effect), $\overline{T'}\left(t\right)$ is the mean temporal deviation of the temperature throughout the measures (synoptic effect), $\widetilde{T}\left(\vec{x},t\right)$ are the local spatial deviations that change throughout the time and ε a local instrument error when measuring the temperature. The decomposition was made from $\widetilde{T}\left(\vec{x},t\right)$ (Lundquist *et Al.*, 2008)

Once decomposed the temperature series, some useful thresholds were found. Using these, the whole AWS were classified in function they are in a probably CAP area or not.

- *First Principal Component (PC1)*

Applying the singular value decomposition (SVD) the first principal component was obtained, which represents the 39.76% of the variance.

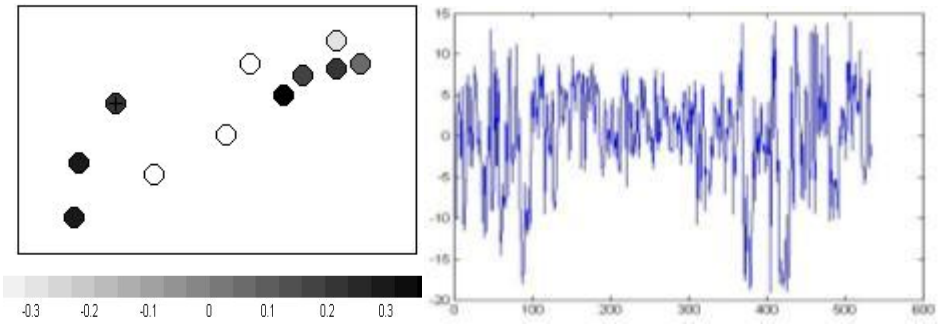

Figure 4. Left) EOF weights' spatial distribution across the space; Right) PC1 temporal serie

Since HMAWS (white points within figure 4 left) had negative weights and the other AWS had them positive or near zero, then there is a huge possibility that the PC1 is related to CAP events. A rigorous way to confirm this idea was to relate the PC1 with a meteorological variable. Therefore, it was chosen the NCEP-NCAR reanalysis data (Kalnay *et Al.*, 1996) of 2.5º X 2.5º grid at 700 hPa level (Lundquist i Cayan, 2007), as it is considered the free air level closer to the highest peaks in the Pyrenees.

- *elationship PC1-free atmosphere: CAP formation*

The correlation was calculated between the PC temporal series with different meteorological variables at 700 hPa: geopotential height (H700), temperature (T700), relative humidity (RH700) and scalar wind velocity

As seen in table 3, the correlation values obtained in the cold months lead to think about the relationship between PC1 and the CAP events.

Finally, comparing the temporal evolution of the time series of PC1 (Figure 5) the oscillations are stronger in the cold months than in the warm ones, explained by the more frequent pass of cold fronts and CAP*R* formation. (Whiteman *et Al.*, 1999; Neff and King, 1989).

| | $R^2$ TOTAL | $R^2$ COLD | $R^2$ HOT |
|---|---|---|---|
| **PC1 vs. H 700** | 0.19 | **0.53** | 0.22 |
| **PC1 vs. T 700** | 0.06 | **0.33** | 0.16 |
| **PC1 vs. RH 700** | 0.23 | 0.30 | 0.19 |
| **PC1 vs. MV 700** | 0.14 | 0.18 | 0.10 |

Table 3.

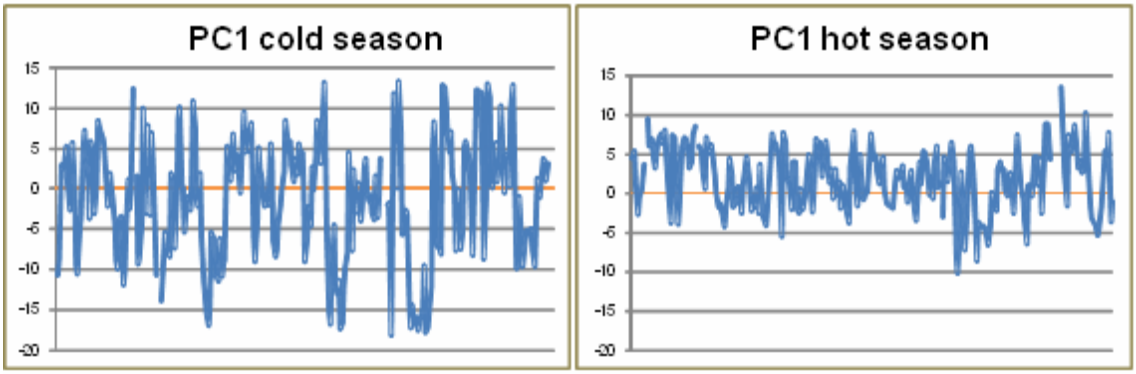

Figure 5. PC1 cold period (left) and warm period (right)

- *Determining CAP zones*

Following the indications given by Lundquist *et Al.*, 2008, to discriminate whether CAP, NO-CAP or indeterminate sites a threshold of one standard deviation was chosen for the EOF. In this case, the weight obtained as threshold was the following:

| | CAP | NO-CAP | Indeterminate |
|---|---|---|---|
| **EOF** | > 0.23 | < -0.23 | -0.23 ≤ x ≤ 0.23 |

Hence, the AWS within the Segre River valley were classified:

| | | |
|---|---|---|
| W5 | **0.2808** | **CAP** |
| CJ | **0.2893** | **CAP** |
| CD | 0.2146 | Indeterminate |
| DP | **0.3602** | **CAP** |
| Puigc | 0.1601 | Indeterminate |
| Estavar | 0.1984 | Indeterminate |
| EyneMus | 0.0275 | Indeterminate |
| ftRCows | **-0.3103** | **NO-CAP** |
| Z9 | **-0.3965** | **NO-CAP** |
| Z3 | **-0.4090** | **NO-CAP** |
| Z8 | **-0.4169** | **NO-CAP** |

The HMAWS do obtained the negative values lower than -0.23 and these were considered to be out of CAP sites, so NO-CAP.
The other AWS had positive EOF, although only three ones (DP, CJ i W5) exceed 0.23 which indicated that these are in CAP sites, the others (CD, Puigcerdà, Estavar i EyneMus) had no-signal values and made them indeterminate.

### *4.2 Dynamic methods*

The intention of this step was to understand the air dynamics and its influence on the temperature factor in complex terrain areas.

*Methods based on DEM*

- *Cold air cumulative potential areas (Lundquist et al, 2008)*

Some orography shapes determine the accumulation of cold air. So, the CAP events are more likely in concave and flat zones enclosed by higher areas.

In order to determine these areas a 200 m DEM was used. A surface map of slope was obtained, also the rank elevation of each pixel relative to the elevation of surrounding pixels within the square with the specified radius in each cardinal direction from the pixel was calculated to identify local ridges or valleys, and finally the curvature within the user-defined radius .
Then, the map showed the probability of cold air accumulation (Figure 6).

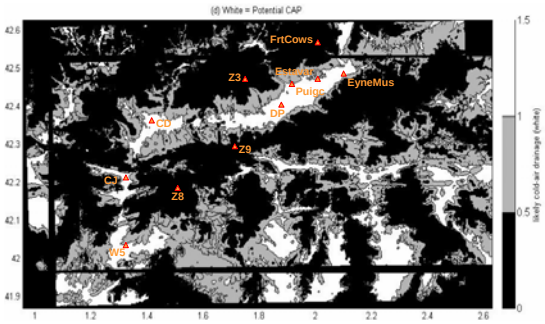

Figure 6.

However, the results obtained with the DEM to determine the CAP areas are not enough as drainage and local circulation can act within the main valley and the tributaries.

Therefore, the study was completed with drainage tools in order to take into account the air circulation behavior within complex orography zones.

- *"Topographic Amplification Factor" ( TAF )*

The *Topographic Amplification Factor* (TAF) (Steinacker, 1984; McKee and O'Neal, 1989; Whiteman, 1990) is a technique used to determine where the cold air is prone to accumulate or drains in clear and calm nights due to high atmospheric pressure and weak pressure gradient.

The cooling rates are bigger in a valley than in adjacent plain, thus depending on the width of the valley will be different cooling rates for the cross sections along the valley. These amplitudes will determine the air circulation along the valley and these are quantified by the TAF:

$$TAF = \frac{\left[\frac{W}{A_{yzvalley}}\right]}{\left[\frac{W}{A_{yzplain}}\right]} = \frac{\left[\frac{W}{A_{yzvalley}}\right]}{\left[\frac{1}{H}\right]}$$

where $W$ is the valley top width, $A_{yz}$ is the cross-section area of the chosen valley, and $H$ is the height of the valley cross-section, from the lower point of the cross-section to $W$ level.

When the TAF decreases downward, it means that a horizontal pressure gradient is created producing down-valley winds, so drainage. On the other hand, when TAF increases in such direction, there is air stability and CAP is able to form (McKee and O'Neal, 1989; Whiteman, 1990).

In order to calculate the TAF along the Segre River valley, 7 cross-sections were chosen (figure 7) trying to include the AWS used in the study.

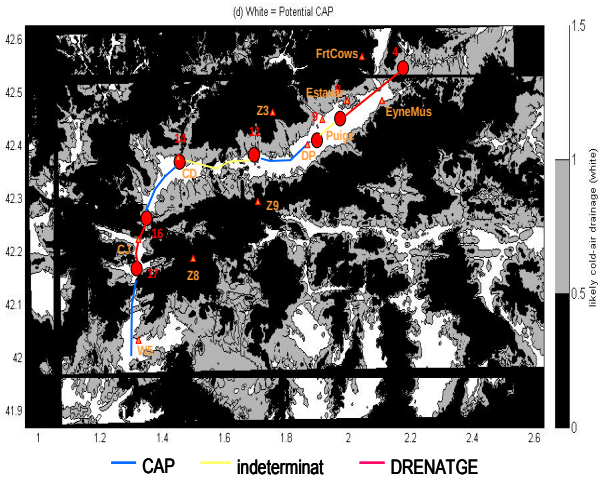


Figure 7. Depending on TAF: CAP (blue), NO-CAP (red) and indeterminate (yellow)

The TAF gave us a good approximation to the reality, but due to the complexity of the Segre River Valley, with their basins, canyons and tributaries, it was needed to refine the results using a drainage model.

## *Drainage Model*

- *Description (Sievers, 2005)*

The single-layer numerical model that calculates the depth and the mean wind of a surface based stable layer that evolves from a neutrally stratified atmosphere during nigh time. The model uses a vertically averaged momentum tendency equations for the velocity and direction of the cold air drainage, in the other hand the changes in the total heat deficit in the cold air layer are calculated from a prescribed local heat loss rate (describing turbulent and radiative cooling) and advection (donor-cell algorithm). The depth of the cold air layer (depth of the surface based temperature inversion) is calculated diagnostically from the total heat loss deficit. The model is initialised with neutral stratification at sunset (onset time of nocturnal cooling).

The configuration used was a grid of 824x1372 with a horizontal resolution of 50 meters that contains in every point the information of terrain height and land uses (9 types). The simulation ranges from the sunset to the dawn, 12 hours.

The wind appearing in each figure with arrows is vertically averaged over the depth of the cold air layer. The colors painting the simulations show the flow intensity.

- *Results*

To verify the KLAM_21 simulations, a winter synoptic situation characterized by either light wind or calm, sky clear, was chosen. The 22nd December 2005 synoptic chart showed a surface high pressure on the southwest of Europe (1032 hPa) (Figure 8).

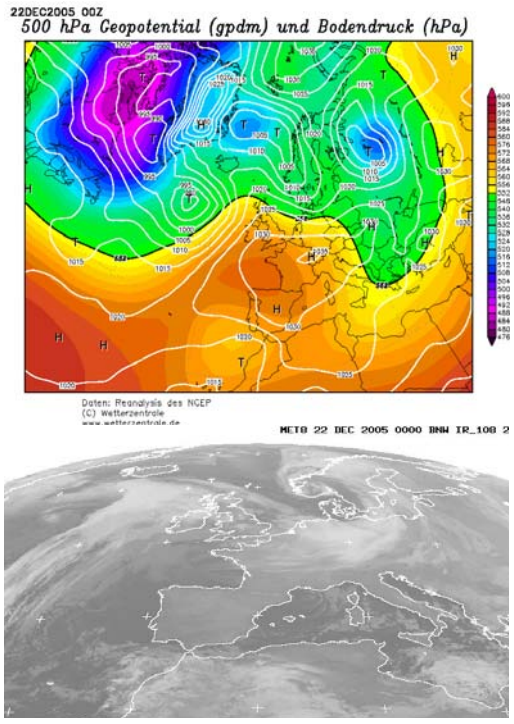


Figure 8. Synoptic surface chart (left); IR Meteosat image (right)

To study thoroughly the valley, the main basins within the Segre River valley were analyzed with the help of some AWS.

*Oliana basin*:

This basin is located in the southern stretch of the valley, after the last canyon and a dam wall, and composed by a flat bottom basin surrounded by mountains around 1000 m high (Figure 9).

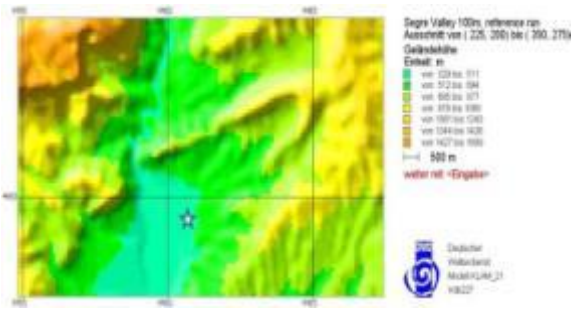

Figure 9. KLAM_21 Oliana basin topography (200 m). W5 AWS (white star)

The KLAM_21 simulation (Figure 10) shows a moderate wind (2-5 m/s) running along the Segre River Valley, especially in the dam wall area and in the canyon which increase along the night. After the sunset, the north-eastern tributary show drainage flows which finally converge with the moderate wind flowing downslope and downvalley in the middle of the river valley. This initial convergence leads a cold air pooling up-valley from the area where tributary merge with the Segre valley.

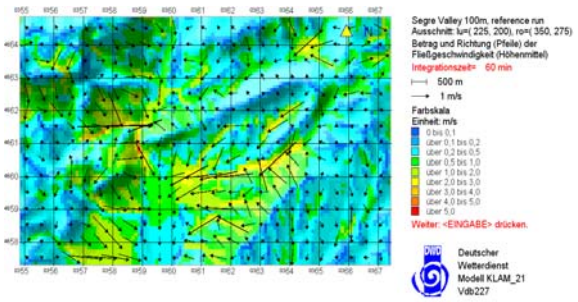

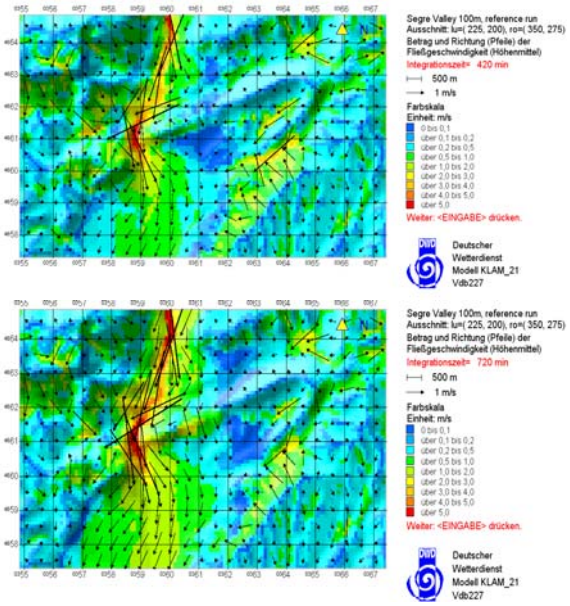

Figure 10. Wind direction and wind speed simulation. 60', 420' i 720' since the sunset.

*Organyà basin*:

This basin is located in the gorges area existing along the studied valley, surrounded by peaks higher than 1400 meters and some tributaries due to steep slopes around there (Figure 11).

Not only this basin is influenced by the Segre River valley, but also by the Cabó valley, perpendicular to the main one oriented from the west to east.

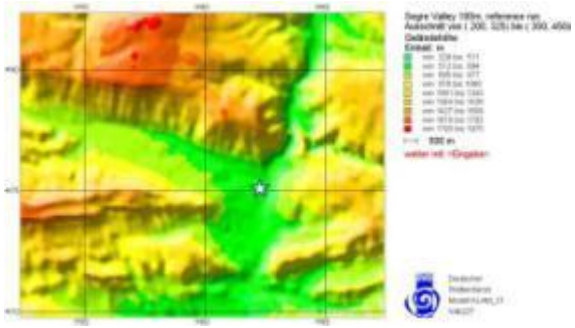

Figure 11. KLAM_21 Organyà basin topography (200 m). CJ AWS (white star)

The first KLAM_21 model simulation showed several tributaries merging to the main valley which after the sunset (Figure 12) drain with moderate speed flow down-valley, especially the Cabó valley.

The model shows as the hours go by that the flows getting into the basin are more variables and the wind speed decreases, and even the wind reach the calm.
It is interesting that the area of Cabó achieve the calm winds or the lighter ones

up-valley as the drainage flows are blocked by the down-valley wind along the Segre River Valley.

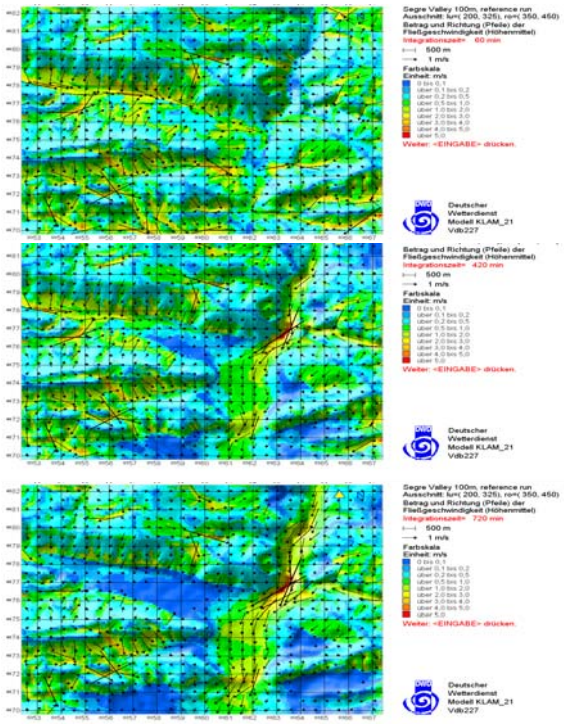

Figure 12. Wind direction and wind speed simulation. 60', 420' i 720' after the sunset.

*Ribera d'Urgellet basin:*

The Rivera d'Urgellet basin is located in an elbow of the Segre River Valley, and it is surrounded by mountains ranging from 1000 to 1600 m. The basin had two main tributary valleys: The Segre Valley and the La Valira Valley (Figure 13)

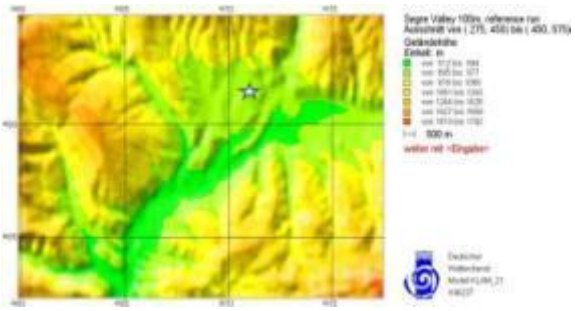

Figure 13. Seu d'Urgell and Ribera d'Urgellet basin

After the sunset, the KLAM_21 simulation (Figure 14) shows moderate drainage from all the tributary valleys as also at the main valley. As the time passes, the basin fills up with cold air and the wind speed decreases but only in the tributaries. The main valley shows drainage in the axis all the night, but the wind calms along the riverside in this area and there is some cold-air pooling. Therefore, at the higher areas of the basin there are no CAP events since the cold air mass is very shallow and the drainage is possible.

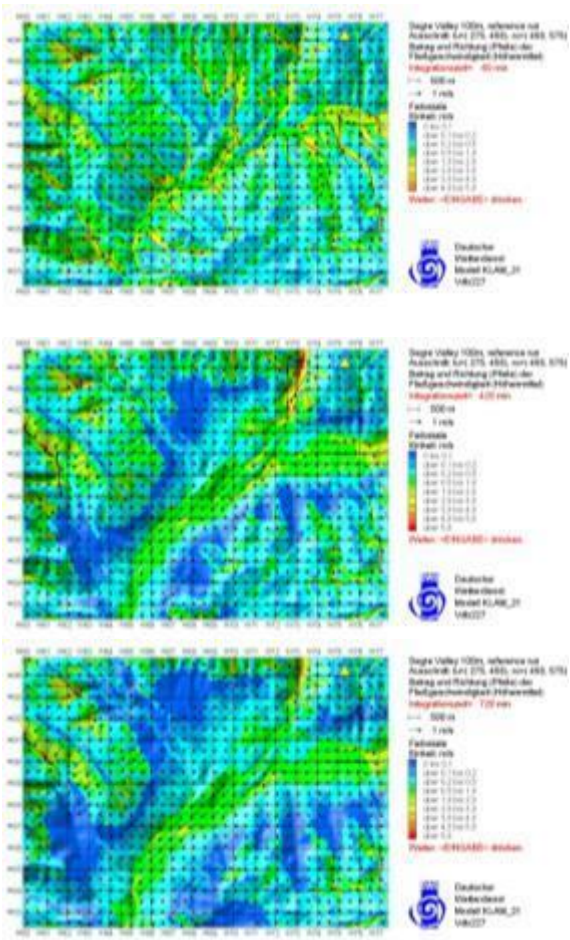

Figure 14. Wind direction and wind speed simulation. 60', 420' i 720' after the sunset.

*Cerdanya basin:*

The Cerdanya basin (Figure 15), characterized by Das AWS (DP), is the widest one, limited by the Pyrenees in the north and the south, with peaks over 2000 m high. This basin is also featured by its orientation, from NE to SW, and many tributary valleys. The main tributaries are the Carol Valley that comes from the cold area of Conflent in the north face of the Pyrenees range, the Osseja Valley with the Puigmal Peak (2910 m) and the plateau in the northeastern area, the French Cerdagne.

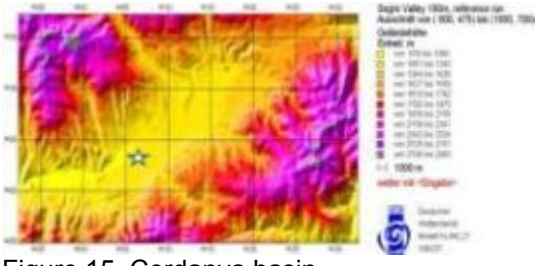

Figure 15. Cerdanya basin

The KLAM_21 simulations (Figure 16) show strong katabatic winds downvalley and downslope along the basin one hour after the sunset. After three hours the model shows air accumulate near the narrow gorge where the Cerdagne basin closes and six hours later, this fact is more evident. Moreover, the drainage model shows how the cold air fills progressively the bottom valley since either calm or weak winds are represented.

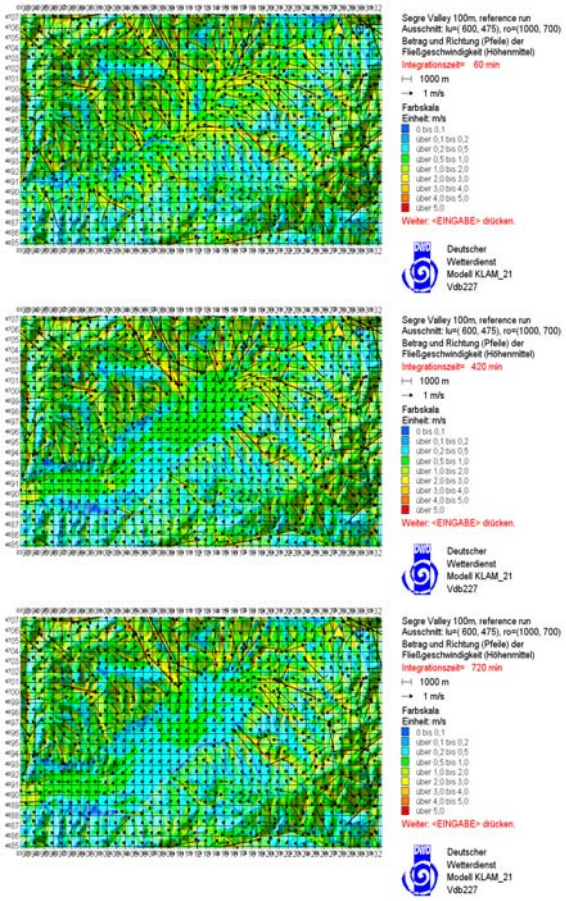


Figure 16. Wind direction and wind speed simulation. 60', 420' i 720' after the sunset.

## 5. CONCLUSIONS

Firstly, from the correlation analysis a first separation among the AWS was obtained. The HMAWS separated clearly from the rest since present high and homogenous correlations. On the other hand, BVAWS and IAWS had the lower and the more heterogeneous correlations among them, despite their proximity. However, some of them were a little bit more correlated to the HMAWS, such as Eynemuss, Estavar, Puigcerdà and CD. Oppositely the BVAWS (DP, CJ and W5) were the less correlated with HMAWS.

Secondly, the clusters confirmed the results obtained by the correlations when the first separation corresponded suddenly to the HMAWS and to the other kind of stations. Later the other AWS separated with results similar to the correlations but was remarkable DP whose separation was sooner than the other AWS.

The EOF analysis showed the first classification of the AWS related to the CAP probability by means of the prior threshold obtained with the EOF1 and the PC1. The HMAWS were classified to be located on sites without cold-air pooling, some BVAWS (DP, CJ and W5) can register CAP and IAWS and others bottom valley AWS were classified as indeterminate (Eynemuss, Estavar, Puigcerdà and CD).

Hence, using the statistical tools, especially EOF, it was deduced:

1) The CAP formation is not possible at the HMAWS and the homogeneity of the correlations shows a similar behavior for all the sites situated whether below 1800 m over the bottom valley. The strong relation among this sort of AWS is surely related on the influence of the free atmosphere and both synoptic and mesoscale models can be useful in temperatures forecast.

2) The majority of BVAWS are orography-depending and therefore becomes prone to CAP; some others become as indeterminate as IAWS, since these ones have significant correlation with HMAWS and some with BVAWS.

Then, using the dynamic tools, such as DEM, TAF and a drainage model it was deduced:

1) The high mountain areas in the study area are too steep to show CAP events.

2) The bottom valley zones showed three possibilities depending on the orography and the shape of the basins and canyons. Thus the cold-air pooling occurs in either wide or flat or closed basins and also where the valleys narrow.
The drainage, with no likelihood of CAP, occurs within canyons and narrow areas, where the narrow areas widen and on slopes along the valley.
Moreover, depending on the tributaries and the temperature inversion height, the cold air pools or drain in some areas within the basins. So, the dynamic methods also

classify no trend areas (indeterminate) as the statistical methods did.

Summarizing these conclusions a topographic map of the Segre River Valley and surroundings was painted showing the likely CAP, NO-CAP and indeterminate areas obtained by means of the methods employed (Figure 17).

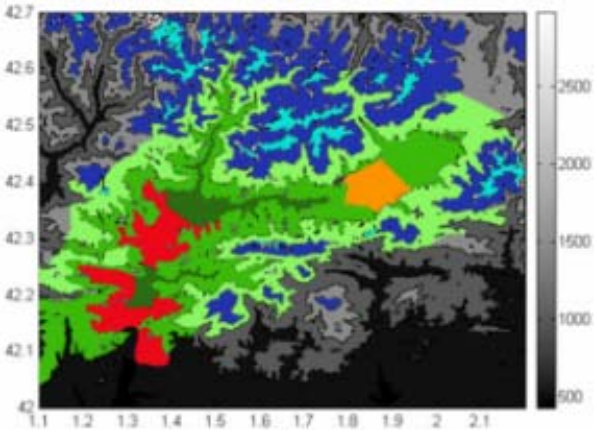


Figure 17. Segre River Valley topographic map. NO-CAP (blue); CAP (orange and red); indeterminate (green)

Finally, due to the indeterminate zones it would be interesting to carry out some experimental and field campaigns and run microscale numerical simulations to understand the cold air behavior in these zones. Moreover, it would be interesting to find the boundary between the height mountain and the lower layers in order to study the temperature inversions.

6. REFERENCES


Kalnay, E., et Al., 1996: The NCEP/NCAR 40-Year Reanalysis Project. Bull. Amer. Meteor. Soc., 77, 437–471.

Lundquist, J. D. and D. R. Cayan, 2007. Surface temperature patterns in complex terrain: daily variations and long-term change in the central Sierra Nevada, California. *J. Geophys. Res*., 112, D11124,

Lundquist, J. D., Pepin, N. C, and Rochford, 2008: Temperature trends at high elevations: Patterns across the globe, *Geophysical Research Letters, 35*

McKee, T. B., and R. D. O'Neal, 1989: The role of valley geometry and energy budget in the formation of nocturnal valley winds.
J. Appl. Meteor., 28, 445–456.

Neff, W. D., and C. W. King, 1989: The accumulation and pooling of drainage flows in a large basin. J. Appl. Meteor., 28, 518–530

Pagès M., Miró, J.R., 2009: Determining temperature lapse rates over mountain slopes using vertically weighted regression: a case study from the Pyrenees. Meteorological Applications, volume 17, issue 1, pages 53-63

Steinacker, R., 1984: Area-height distribution of a valley and its relation to the valley wind. Contrib. Atmos. Phys., **57**, 64-71.

Uwe Sievers, 2005: Das Kaltluftabflussmodell KLAM 21, Berichte des Deutschen Wetterdienstes 227

Whiteman, C.D.,1990: Observations of thermally developed wind system in mountainous terrain. Atmospheric Processes over complex terrain, Meteor. Monogr., No. 45, Amer. Meteor. Soc., 5-42

Whiteman,C.D., X. Bian and S. Zhong, 1999: Wintertime evolution of a temperature in the Colorado Plateau Basin. J. Appl. Meteor., 38, 1103-1117

Whiteman, C. D., 2000: *Mountain Meteorology. Fundamentals and Applications.* Oxford University Press